crystals

MDPI

Article

Assessment of Physicochemical, Anticancer, Antimicrobial, and Biofilm Activities of N-Doped Graphene

Abdulaziz Alangari [1], Fahad M. Aldakheel [1], Ayesha Mateen [1], Mohammed S. Alqhatani [2], Ahmed L. Alaofi [2], Mudassar Shahid [2], Raisuddin Ali [2], Rabbani Syed [2,*], Syed Farooq Adil [3], Mujeeb Khan [3], Mufsir Kuniyil [3] and Mohammed Rafi Shaik [3,*]

[1] Department of Clinical Laboratory Sciences, College of Applied Medical Sciences, King Saud University, P.O. Box 10219, Riyadh 11433, Saudi Arabia; aalangari2@ksu.edu.sa (A.A.); faldakheel@ksu.edu.sa (F.M.A.); amateen.c@ksu.edu.sa (A.M.)

[2] Department of Pharmaceutics, College of Pharmacy, King Saud University, P.O. Box 2457, Riyadh 11451, Saudi Arabia; msaalqahtani@ksu.edu.sa (M.S.A.); ahmedofi@ksu.edu.sa (A.L.A.); mahmad1@ksu.edu.sa (M.S.); ramohammad@ksu.edu.sa (R.A.)

[3] Department of Chemistry, College of Science, King Saud University, P.O. Box 2455, Riyadh 11451, Saudi Arabia; sfadil@ksu.edu.sa (S.F.A.); kmujeeb@ksu.edu.sa (M.K.); mkuniyil@ksu.edu.sa (M.K.)

* Correspondence: rsyed@ksu.edu.sa (R.S.); mrshaik@ksu.edu.sa (M.R.S.); Tel.: +966-11-46-70439 (M.R.S.)

Abstract: Nanomedicine has been used as a precise treatment for many diseases. The advantage of using nanodrugs is that they have more permeability and less toxicity to cells, which enhances the drug delivery system. Graphene is well known for its potential biological applications in drug, food, and pharma industries. This study aimed to assess the productivity and potentiality of nitrogen-doped graphene (NDG) and to evaluate their anticancer, antimicrobial, and biofilm inhibition activity. Nitrogen-doped graphene was synthesized by using a one-pot facile synthesis of NDG, wherein the NDG was prepared by the reduction of graphene oxide (GO) in the presence of hydrazine hydrate as a reducing agent, while ammonium hydroxide was used as a source of nitrogen on the surface of graphene. As-synthesized NDG was characterized by various characterization techniques such as UV-Vis, FT-IR, XRD, XPS, TEM, and N_2 sorption studies analysis. Antimicrobial, anticancer, and biofilm inhibition assays were performed by standard protocols. N-doped graphene (NDG) showed better activity against Gram-positive bacteria, such as methicillin-resistant *Staphylococcus aureus* (MRSA), *Bacillus subtillis*, *Streptococcus pneumoniae*, and *Streptococcus mutans* ($p \leq 0.05$), whereas there was no activity against Gram-negative strains in *Klebsiella pneumoniae* and *Pseudomonas aeruginosa*. Biofilm inhibition was also improved with NDG compared to the standard ampicillin. NDG showed better results in both MCF-7 and Hela cell lines with IC_{50} of 27.15 µg/mL and 30.85 µg/mL, respectively. In conclusion, NDG has the best ability for use as a biomolecule, and research studies focusing on proteomics, metabolomics, and in vivo studies are needed to increase the impact of NDG in the drug and pharma industry.

Keywords: graphene; nitrogen; anticancer; physicochemical; antimicrobial; biofilm

Citation: Alangari, A.; Aldakheel, F.M.; Mateen, A.; Alqhatani, M.S.; Alaofi, A.L.; Shahid, M.; Ali, R.; Syed, R.; Adil, S.F.; Khan, M.; et al. Assessment of Physicochemical, Anticancer, Antimicrobial, and Biofilm Activities of N-Doped Graphene. *Crystals* **2022**, *12*, 1035. https://doi.org/10.3390/cryst12081035

Academic Editor: Conrad Becker

Received: 1 July 2022
Accepted: 20 July 2022
Published: 26 July 2022

1. Introduction

Many diseases that were previously thought to be incurable have now been successfully treated. Even though there are obstacles to overcome, the rapid growth of target-based anticancer drugs has provided the opportunity to selectively destroy tumor cells located deep within tissues [1]. Cancer therapies such as chemotherapy, hormonal therapy, and monoclonal antibody therapies are already in use in the clinic. However, they have significant limitations, such as relative ineffectiveness in certain types of cancers or serious side effects that disqualify them from being considered safe drugs. The development of novel

target-based anticancer drugs allows for the selective targeting and eradication of cancerous cells [2,3]. Advanced methods have been used, such as the selective accumulation of nanodrugs by modifying their physicochemical properties or the use of human stem cells. However, the use of these nanodrugs resulted in toxicity and was insufficiently effective considering the side effects caused using nanoparticles. Recent research has focused on developing a novel immunotherapeutic strategy that effectively directs immune cells to react against invasive cancer cells [4].

For decades, antibiotics have been used to treat microbial infections. However, antibiotic resistance (AMR) has increasingly been reported locally and globally, leading to extremely high medical costs, reducing immunity, prolonging hospital stay, and high mortality rates [5]. A recent study from Saudi Arabia has reported the emergence and dissemination of colistin resistance among major Gram-negative pathogens, such as *Klebsiella pneumoniae* and *Pseudomonas aeruginosa* [6]. Such a spread of colistin resistance represents a major challenge to public health given that colistin is usually used to treat infections caused by multidrug-resistant (MDR) bacteria, which can complicate the therapeutic options available for clinicians to manage patients. To combat this threat, it is crucial to develop better alternative agents that can reduce the resistance burden and enhance better antimicrobial activity [7].

Biofilms are formed as an aggregate of at least one kind of microorganism that can develop on various surfaces by producing an extracellular polymeric matrix. The phenomenon of biofilm formation on the surface occurs in four stages. It is initially attached to the surface and may be reversible or irreversible after that maturation stage using the EOS matrix. This will develop micro- or macro-colonies. The maturation stage is very crucial, showing differences in susceptibility [8].

Graphene and graphene oxide and their derivatives attract the scientific community's attention due to their remarkable physicochemical properties [9], mainly in biomedical applications where the graphene atom has a high surface area compared to weight; an important functional property to be considered [10]. To date, many scientists have investigated oxidation functional groups of graphene, which can be utilized to discover different compound materials, showing extraordinary improvement in biological, physical, and chemical characterization used in combination with different nanocomposites [11]. Along with the positive impact of graphene nanoformulations, some studies were reporting negative aspects of graphene that can lead to cell death due to inflammation, which is purely dependent on the type of treatment, duration of exposure, and concentration used [12]. Our main objective of the study was to understand the enhancement of nitrogen-doped graphene and its efficacy as an anticancer and antimicrobial potential towards tested cell lines and microorganisms in association with the physicochemical properties analyzed (Scheme 1).

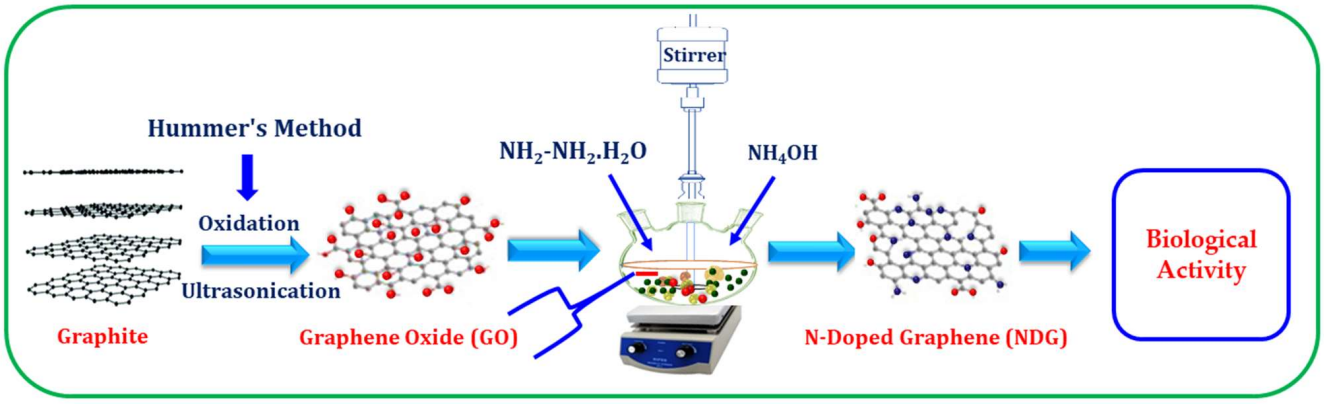

Scheme 1. Graphical representation of as-synthesized NDG, and the evaluation of their biofilm inhibition, antimicrobial, and anticancer activity.

2. Materials and Methods

2.1. Materials

Graphite powder (99.999%, 200 mesh) was purchased from Alfa Aesar (Tewksbury, MA, USA). Ammonia hydroxide solution (NH_4OH), hydrazine hydrate (N_2H_4), sulfuric acid (H_2SO_4, 98%), potassium permanganate ($KMnO_4$, 99%), sodium nitrate ($NaNO_3$, 99%), and hydrogen peroxide (H_2O_2, 30 wt%), all organic solvents, were obtained from Aldrich Chemicals (St. Louis, MO, USA) and were used directly without further purification.

2.2. Synthesis of Graphene Oxide (GO)

The modified Hummers method [13] was used to prepare GO from bulk graphite powder procured from Alfa Aesar (USA) chemicals. To begin, 0.5 g of 99.999% pure graphite powder with 200 mesh specification was added to 23 mL of conc. H_2SO_4 and 0.5 g of $NaNO_3$ were placed in an ice bath under stirring. To stir the ice-cold solution, 3 g of $KMnO_4$ was added slowly. After adding the $KMnO_4$ to the reaction mixture, the solution was stirred for 1 h in a water bath of temperature 35 ± 5 °C to form a thick green paste. Deionized water measuring 40 mL (DI) was added very slowly to the green paste formed and the temperature increased to 90 ± 5 °C in a 30 min period. In the last step, 100 mL more of deionized water (DI) followed by 3 mL H_2O_2 was added to turn the color from dark brown to yellow. The obtained product was filtered while warm using Whatman filter paper grade 1 and washed many times until the pH was ~7. The final product is dispersed in deionized water (DI) in a ratio of 5 mg in 1 mL deionized water (DI).

2.3. Synthesis of N-Doped Graphene (NDG)

In this method, GO was used as the starting material. GO (100 mg) synthesized using the Hummers method was dispersed in deionized water (20 mL) by ultrasonication method. The dispersion was then collected in a round bottom flask, to which 4 mL of NH_4OH and 4 mL of hydrazine hydrate were added simultaneously; here, ammonium hydroxide acting as the source of nitrogen. The reaction flask was equipped with a condenser, and the dispersion was allowed to stir for 3 h at 90 °C in a water bath. After 3 h of stirring, the reaction vessel was allowed cool to reach RT and centrifuged the products at 8000 rpm. The precipitate was washed many times with distilled water and dried at 65 °C for 12 h.

2.4. Screening of Synthesized NDG for Antimicrobial Analysis

The agar diffusion technique was adopted to test the antimicrobial activity of the synthesized NDG. The microbial strains were selected from the global priority pathogens (GPP) list as we have analyzed in our previous study. Selected microbial cultures were procured from the microbiology department, College of Pharmacy, King Saud University, Riyadh. The glycerol stock cultures of six bacterial strains (*Klebsiella pneumoniae*, *Pseudomonas aeruginosa*, methicillin-resistant *Staphylococcus aureus* (MRSA), *Bacillus subtillis*, *Streptococcus pneumoniae*, and *Streptococcus mutans*) were taken and initially cultured on Muller Hilton agar media and monitored for isolating pure colonies for further antibacterial susceptibility testing [14]. In brief, pure colonies were selected from each microbial strain and cultured on Mullar Hilton broth at 37 °C for 24–48 h incubation. Next, 0.5 McFarland standard culture was prepared, and the broth was spread onto the Mullar Hilton agar plates by using the sterile spreader. A standard antibiotic stock and NDG concentrations were freshly prepared, and the working stock was prepared from the stock (ampicillin 100 µg/mL) for bacterial strains and NDG 100 µg/mL. Sterile blank discs were impregnated with a defined concentration of an antimicrobial agent and NDG and one blank broth disc as a positive control was placed on the surface of an agar plate. The plates were incubated and the zone of inhibition showing susceptible or resistance results was analyzed by measuring the diameter of the inhibition zone using a ruler. The entire analysis was performed in triplicate.

2.5. Screening of Synthesized NDG for Biofilm Activity

The antibiofilm activity of the NDG was assessed using a static microtiter plate assay. Briefly, an overnight culture of MRSA and *Pseudomonas aeruginosa* strains was diluted using Tryptic Soy Broth (TSB) and supplemented with 1% glucose, 100 µL of the culture containing 1.5×10^8 CFU/mL was added to a 96-well Costar polypropylene plate, and NDG 100 µL was added to one well from the stock solution (1 mg/mL) and was two-fold serially diluted using the TSB to obtain concentrations of 100, 50, 25,12.5, and 6.25 µg/mL, and standard antibiotic ampicillin 1000 µg/mL and gentamycin 200 µg/mL concentrations were used and serially diluted to obtain the minimum concentration of the antibiotic to evaluate antibiofilm activity.

After overnight growth, the planktonic cells were washed away with deionized water and the remaining adhered biomass was stained with 0.1% crystal violet, washed with water, and solubilized in 30% acetic acid. Total biofilm mass was quantified by measuring the optical density (OD) at 595 nm using a microtiter plate reader. The percent biofilm inhibition was calculated in relation to the amount of MRSA biofilm grown in the absence of NDG (defined as 100%) and the media sterility control (defined as 0% growth). Results from three separate biological replicates were averaged.

2.6. Determination of Minimum Biofilm Inhibitory Concentration (MBIC)

One-hundred microliter of bacterial strains *Pseudomonas aeruginosa* and MRSA strains inoculums of 1.5×10^8 CFU/mL TSB culture were incubated for 24 h at 37 °C in polystyrene, round bottom 96-well microplates (Corning, NY, USA). After incubation, the supernatant was aspirated, and the wells were washed twice with sterile normal saline solution. One-hundred microliter of NDG (stock 1 mg/mL) and antibiotics were added to the well and two-fold serially diluted with TSB broth, which was added to the wells with the established biofilms. After incubation for 18 h at 37 °C, MBIC was recorded. MBIC is defined as the lowest concentration of the antibiotic/nanobiotic that results in no visible growth [15].

2.7. Determination of Antibiofilm Activity by Inverted Microscope

After 24 h of incubation at 37 °C, the cells were observed in a 12-well microtiter plate under an inverted microscope (Olympus, Tokyo, Japan) at 40× magnification [16].

2.8. Determination of Cell Cytotoxicity by 2,5-Diphenyl-2H-Tetrazolium Bromide (MTT) Assay

The anti-cell proliferative activity of NDG was investigated using MCF-7 and HeLa cells by assessing their viability by using an MTT assay [17]. The cultures were grown until the exponential phase and were trypsinized and diluted with DMEM to obtain a cell count of 5×10^5 cells/mL. The suspended cells were grown overnight in a microplate containing a 100 µL medium, a fresh medium with different concentrations of NDG (1.56–200 µg/mL) was added after aspirating the previously grown culture. Cultures suspended in an FBS-free DMEM served as a negative control. All drug concentrations and controls for the assay were performed in triplicate.

The cell suspensions were withdrawn, and the wells were cleaned with PBS after 24 h of incubation. Then, 20 µL of MTT solution (at a concentration of 5 mg/mL in PBS) and 80 µL of medium were added and incubated at 37 °C for 4 h. The culture fluid with MTT was then removed, leaving the formazan crystal to precipitate. The crystals were dissolved in 100 µL of DMSO/acetic acid/sodium lauryl sulfate (99.4 mL/0.6 mL/10 g) at room temperature for 15 min. The microplates were observed, and absorbance was measured at 570 nm using a spectrophotometric microplate reader (Synergy HT, BioTek Inst., Winooski, VT, USA). IC_{50} was calculated using GraphPad Prism 5.0 (San Diego, CA 92108, USA).

2.9. Statistical Analysis

A *t*-test was used to compare the results of antimicrobial activity of the synthesized NDG and standard antimicrobials, where $p < 0.05$ is considered a significant result.

3. Results and Discussions

3.1. UV-Vis Analysis

UV-Vis spectroscopy is used to characterize the synthesized NDG. Figure 1 displays the UV-Vis spectra of GO and NDG. GO produces two distinct absorption peaks in the UV-Vis spectrum at wavelengths of about 230 nm and 300 nm corresponding to the π-π* transition of the C=C bond in the aromatic ring and n-π* for C=O bonds [18]. In contrast, NDG displays a shift in peak position from 300 to 283 nm. Peak shifting to a lower wavelength in the UV-Vis spectrum of NDG compared to GO indicates increased bond strengths than the precursor. This is supported by the process of removing most of the oxygenic groups and the restoration of C=C conjugation, leading to the strong bonding nature of electrons [19].

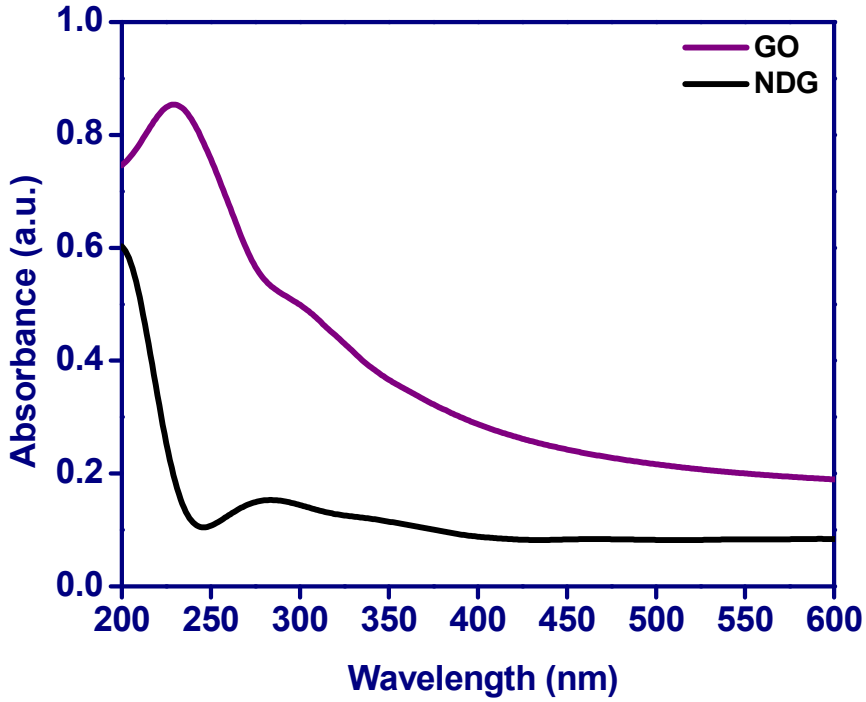

Figure 1. UV-Visible spectra of graphene oxide (GO) and nitrogen-doped graphene (NDG).

3.2. FT-IR Analysis

The functional groups present in the NDG are characterized by FTIR spectroscopy. The comparative data of FTIR spectra for GO and NDG are plotted in Figure 2. Since the GO contains plenty of oxygen groups attached to the graphene layer, numerous signals are produced in the FTIR spectrum, especially in the wavenumber range of 1000–1800 cm^{-1}. The oxygen-to-carbon bonding in GO varies from carbonyl (C=O), hydroxyl (-OH), etheric (C-O-C), and alcoholic (C-O), which produce various vibration signals at 1735 cm^{-1} (stretching), 1400 cm^{-1} (bending), 1224 cm^{-1} (stretching), and 1053 cm^{-1} (stretching), respectively [20]. In addition to the vibration peaks produced by carbon-bonded oxygen atoms, a broad strong band is displayed at 3428 cm^{-1} in the FTIR spectrum of GO, which is produced by the -OH moiety from the absorbed moisture content. During simultaneous reduction and nitrogen doping, most of the oxygen species were removed, which is observed from the reduced intensity of most of the peaks produced by the oxygen-containing groups, especially the oxygen present on the edges. However, a small peak present at 1053 cm^{-1} indicates the presence of traces of oxygen in the NDG. The doping of nitrogen in the graphene sheet is confirmed by the peak at 1154 cm^{-1}, which resonated from the vibrations of the C-N bond [21]. Moreover, the C=C unsaturation of graphene is reverted in the NDG evident from the peak at 1558 cm^{-1} [22]. The wide high intense peak present at 3436 cm^{-1} is possibly due to the N-H stretching vibrations or by the O-H bond as in GO [23].

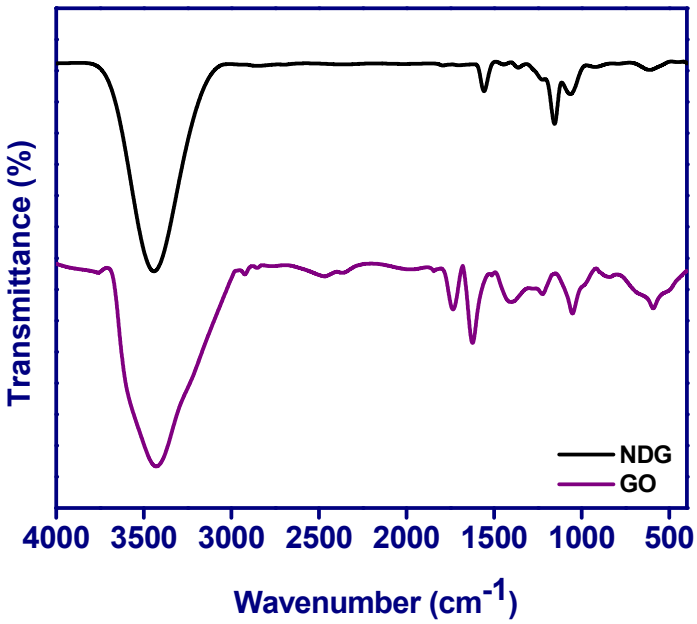

Figure 2. FT-IR spectra of GO and NDG.

3.3. XRD Analysis

The crystal structure of NDG is studied using XRD analysis. The spectral pattern obtained for NDG is compared with the precursors. Figure 3 displays the XRD pattern of graphite, GO, and NDG. Pure graphite exhibits a highly crystalline nature as revealed from the XRD pattern of pure graphite and a sharp peak at 26.5° (002) with a *d*-spacing of 0.34 nm calculated using Bragg's equation [24]. After the oxidation and exfoliation of graphite into GO sheets, the peak shifted to 13.4° (001) with an increased interplanar distance of 0.66 nm. As observed in Figure 3, the diffraction peaks corresponding to graphite (2θ = 26.5°) and GO (2θ = 13.4°) are completely absent in the XRD pattern of NDG. NDG, being a turbostratic material, displays a broad peak at 23.4° corresponding to the (002) plane and a small shoulder at 42.8° corresponding to (004) or (100) planes [25]. The *d* spacing value NDG is calculated as 0.37 nm. The decrease in *d* spacing indicates the restoration of unsaturated conjugation through the removal of intercalated oxygenic functional groups.

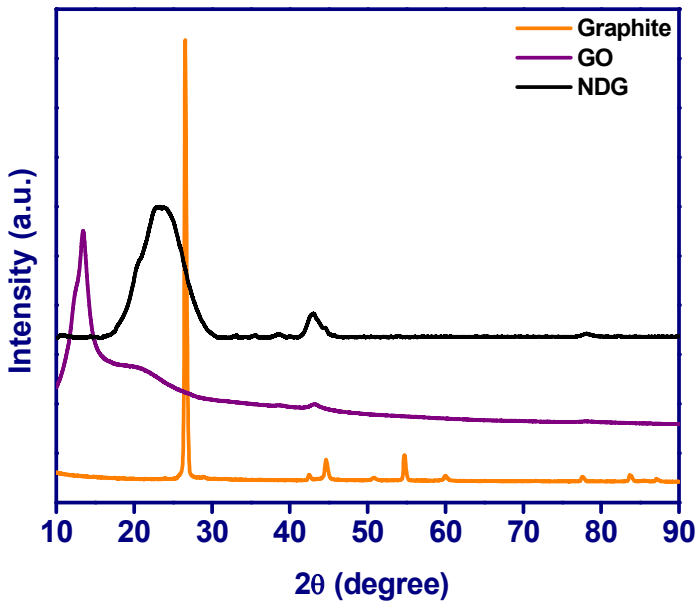

Figure 3. XRD pattern of graphite, GO, and NDG.

3.4. XPS Analysis

XPS analysis was performed to examine the elemental combination of the prepared NDG. Figure 4 shows the full spectra survey obtained for NDG. The presence of exclusive peaks corresponding to carbon, nitrogen, and oxygen indicates that the compound is free from other impurities.

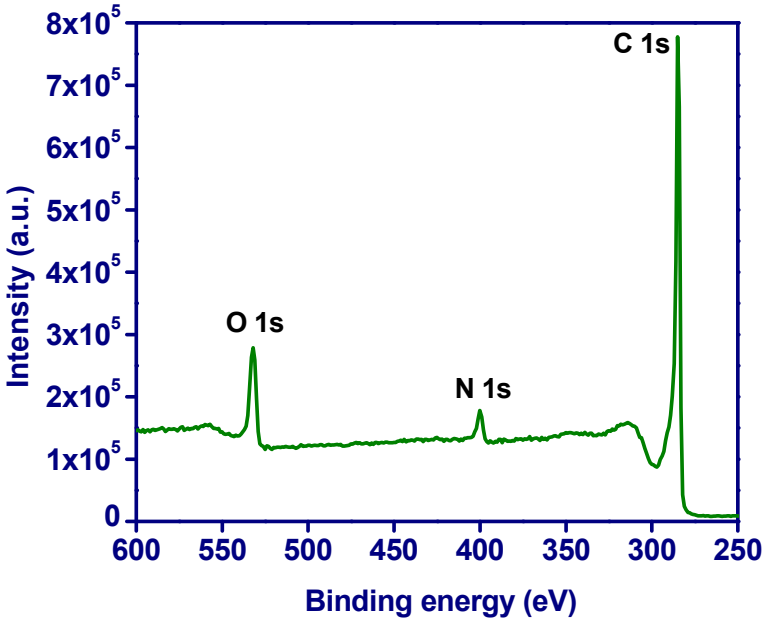

Figure 4. XPS full scan image of NDG.

3.5. N_2 Sorption Studies

N_2 adsorption–desorption isotherm analysis was carried out to investigate the surface and porosity using a surface area and porosity analyzer. Figure 5 shows an adsorption–desorption isotherm measured at a liquid nitrogen temperature of −196 °C. The type IV isotherm, with a characteristic H_2 hysteresis loop, was observed for NDG. The shape of the isotherm predicted cage-like mesopores and the change in desorption value was observed due to the capillary condensation occurring in pores [26]. The specific surface area calculated by the BET method is 485.67 m^2/g for NDG.

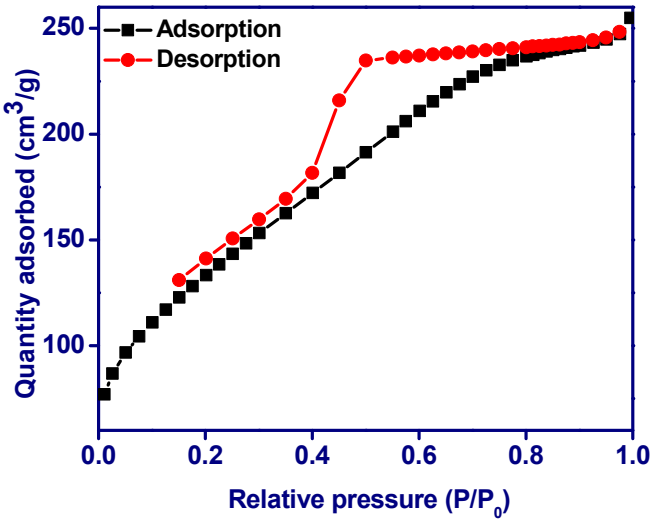

Figure 5. N_2 adsorption–desorption isotherm of NDG.

3.6. TEM Analysis

The detailed morphology and fine structure of NDG are analyzed using TEM. Figure 6 shows the TEM image of the NDG. NDG displays a 2D planar structure with some crumpling in a few areas. The highly transparent nature of the NDG sheets is visible in the image, indicating very few layers are present in the NDG sheets.

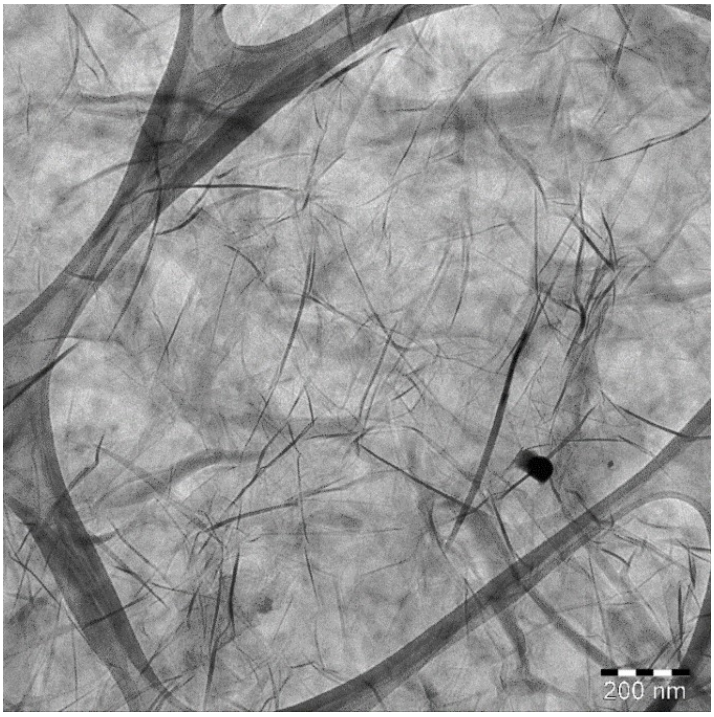

Figure 6. High-resolution transmission electron microscopy (HRTEM) image of NDG.

3.7. Antimicrobial Analysis

The agar diffusion method was used to test antimicrobial susceptibility, and the results are summarized in Table 1. Antimicrobial assessment shows improved results compared to the previous studies. *K. pneumoniae* showed resistance towards NDG with ZOI (14.2 ± 1.86) compared to the standard amplicillin ZOI (19.21 ± 1.39) ($p \geq 0.05$). Similarly, *P. aeruginosa* showed resistance towards NDG with ZOI (17.8 ± 1.98) compared to the standard ampicillin ZOI (19.5 ± 2.75). Gram-positive bacteria, *B. subtillis*, S. *mutans*, S. *pneumoniae,* and MRSA showed susceptibility towards NDG with ZOI (25.12 ± 2.35, 25.7 ± 1.89, 22.31 ± 1.67, 25.45 ± 2.89) compared to the standard ampicllin ZOI (19.22 ± 1.87, 20.3 ± 1.12, 18.21 ± 1.33, 19.16 ± 1.72), respectively ($p \leq 0.05$). As an alternative to antibiotics, NDG is increasingly being used to target bacteria. Although the antibacterial mechanisms of NDG are understood, currently accepted mechanisms include oxidative stress induction, metal ion release, and non-oxidative mechanisms [27]. Pathogenic bacteria are the primary cause of several human infections and pose serious health risks [28]. Since its discovery in 2004, graphene has emerged as a promising nanomaterial due to its unique catalytic, optical, and electrical properties, as well as exceptional physical properties such as a large specific surface area and mechanical strength [29]. Graphene has been found to have promising antibacterial properties in several recent studies [30,31].

Table 1. Zone of inhibitions obtained during agar diffusion test by NDG as compared to ampicillin. Results were presented as mean ± SD, $n = 3$.

Microorganisms	Zone of Inhibitions (mm), Mean ± SD, $n = 3$	
	Ampicillin	**NDG**
Klebsiella pneumoniae	19.21 ± 1.39	14.2 ± 1.86
Pseudomonas aeruginosa	19.5 ± 2.75	17.8 ± 1.98
MRSA	20.3 ± 1.12	24.7 ± 1.89 *
Streptococcus mutans	18.21 ± 1.33	22.31 ± 1.67 *
Streptococcus pneumoniae	19.16 ± 1.72	25.45 ± 2.89 *
Bacillus subtillis	19.22 ± 1.87	25.12 ± 2.35 *

* $p < 0.05$ (Significant).

3.8. Biofilm Inhibition and MBIC Assay Results

The biofilm's inhibition activity has been determined under an inverted microscope (40×), and the difference in the untreated and treated biofilms with antibiotics and NDG could be evaluated clearly by observing the clearance of biofilms and the separation of planktonic cells in comparison with the untreated biofilm (Figures 7 and 8). Previous studies have explored the role of NDG in biofilm inhibition in pathogenic bacteria and provided evidence of metallic nanocomposites acting effectively against biofilm formation [32–35].

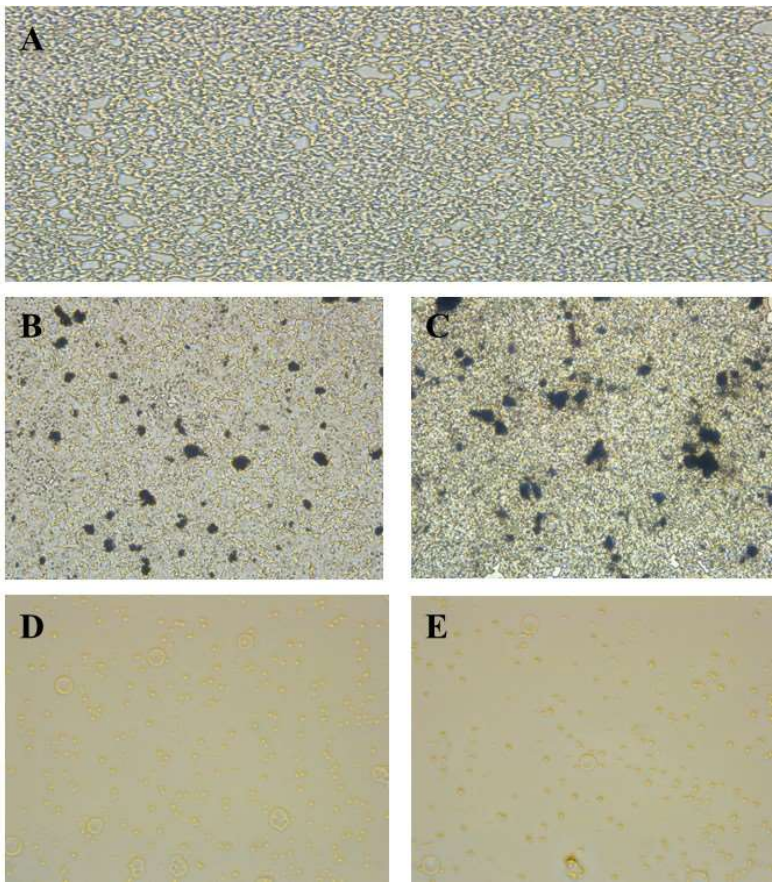

Figure 7. Results observed under an inverted microscope (40×) (**A**). MRSA biofilm untreated, (**B**). MRSA inhibition treated with NDG (100 µg/mL), (**C**). MRSA inhibition treated with NDG (200 µg/mL), (**D**). MRSA inhibition treated with ampicillin (200 µg/mL), (**E**). MRSA inhibition treated with ampicillin (1000 µg/mL).

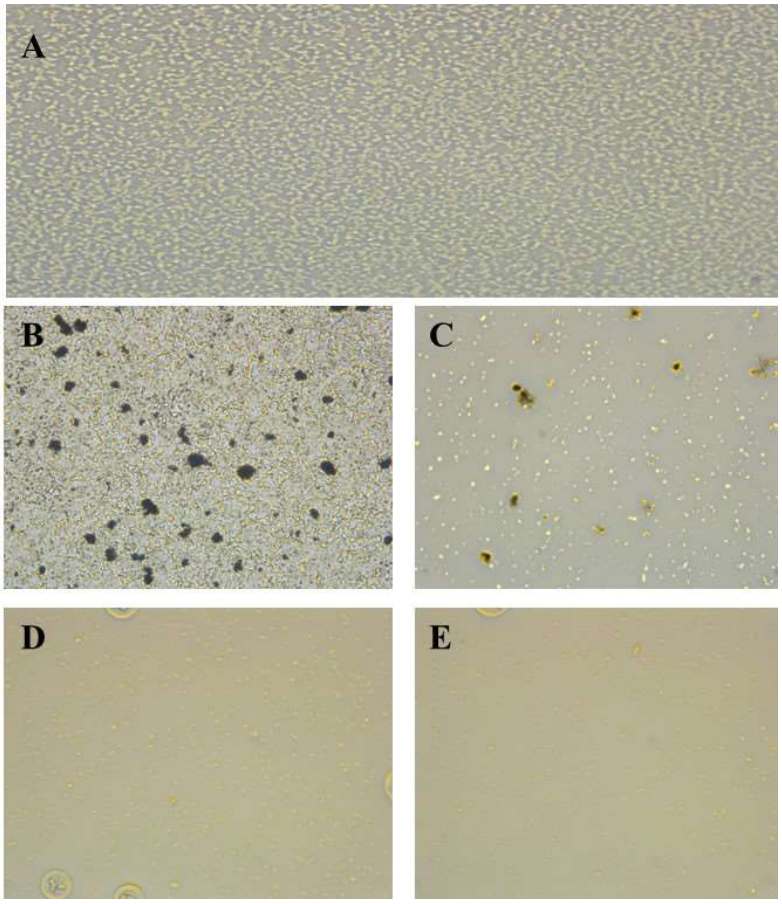

Figure 8. Results observed under inverted microscope (40×) (**A**). *Pseudomonas aeruginosa* Biofilm untreated, (**B**). *Pseudomonas aeruginosa* inhibition treated with NDG (100 µg/mL), (**C**). *Pseudomonas aeruginosa* inhibition treated with NDG (200 µg/mL), (**D**). *Pseudomonas aeruginosa* inhibition treated with ampicillin (1000 µg/mL), (**E**). *Pseudomonas aeruginosa* inhibition treated with ampicillin (2000 µg/mL).

The biofilm inhibition activity of isolates *Pseudomonas aeruginosa* and MRSA has been performed using NDG and has been compared with standard antibiotics ampicillin. The biofilms of *Pseudomonas aeruginosa* and MRSA were found to show a good percentage of inhibition against NDG in contrast to the standard antibiotic ampicillin. The biofilm inhibition activity of NDG against *Pseudomonas aeruginosa* showed the least MIC of 25 µg/mL and showed the highest percentage of inhibition 96.26 with an IC_{50} value of 12.98 µg/mL in comparison to standard antibiotic tested. The results with MRSA biofilm inhibition activities of NDG showing IC_{50} value 23.11 µg/mL with an inhibition percentage of 98.12 in comparison to standard antibiotic-tested results are tabulated in Table 2. Because biofilms are difficult to eliminate, they may increase the risk of infection, lengthen hospitalizations, and boost healthcare expenses. Resistance to antibiotic therapy and gene transfers between bacteria are two mechanisms linked to biofilm protection and survival, which allow the pathogen to dodge host immune responses and create chronic infections [36]. To combat bacterial resistance, scientists are exploring new antibiotic alternatives that not only prevent resistance but also reduce the use of traditional antibiotics, allowing for effective biofilm eradication [37]. Among these, the application of NDG has attracted much attention due to its antibacterial and antibiofilm properties, as revealed in later investigations, and the NDG could be used as an alternative to antibiotics against biofilm-forming bacterial strains [38,39].

Table 2. Evaluation of MIC, percentage inhibition, and IC_{50} values of NDG and Ampicillin.

S. No	Tested Microorganism	Drug	MIC (µg/mL)	Parentage of Inhibition	IC_{50} (µg)
1	*P. aeruginosa*	NDG	25	94.26	12.98
		NDG	50	94.23	26.53
		Ampicillin	1000	90.45	110.55
		Ampicillin	2000	91.31	547.58
2	MRSA	NDG	50	98.12	23.11
		NDG	100	93.76	53.32
		Ampicillin	200	89.79	111.37
		Ampicillin	1000	91.07	137.25

3.9. Cell Proliferation Assay

The percentage cell viabilities of MCF-7 breast cancer cells and HeLa cervical cancer cells against varying concentrations of NDG were represented in Figure 9. Cell proliferation of NDG was examined at 1.56–200 µg/mL, where the observed IC_{50} were 27.15 and 30.85 µg/mL at 24 h against MCF-7 and HeLa cells, respectively. The MTT assay results demonstrate a dose-dependent anti-cell proliferation of NDG against MCF-7 and HeLa. The nanoparticles of herbal drugs tend to augment the anti-cancer potential compared to their native state. Thus, we can assume that NDG can be a potent anti-cell proliferative agent for breast and cervical cancer.

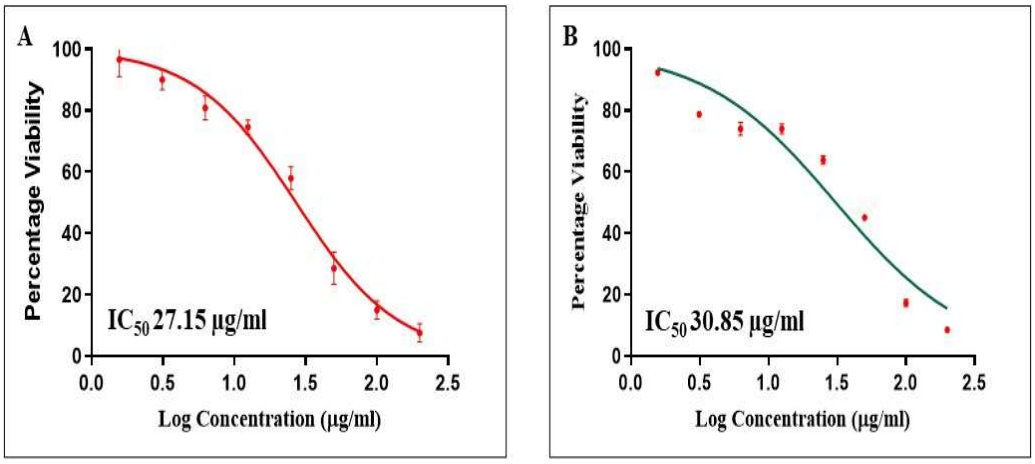

Figure 9. Cytotoxicity after 24 h of incubation with NDG (**A**); MCF-7 cells (**B**) HeLa cells with IC_{50} values (µg/mL).

Nanosystems are in use in successfully carried into tumor cells, causing visible cell death and necrosis; these agents might suppress tumor cell growth with increased efficacy, with accelerated apoptosis and necrotic effects on carcinogenic cells [40].

4. Conclusions

Herein, nitrogen-doped graphene was successfully synthesized by using the one-pot facile synthesis of NDG, wherein the NDG was prepared by the reduction of graphene oxide in the presence of hydrazine hydrate as a reducing agent, while ammonium hydroxide was used as a source of nitrogen on the surface of graphene and also investigated their anticancer, antimicrobial, and biofilm inhibition activity. NDG exhibited better activity against methicillin-resistant *Staphylococcus aureus* (MRSA), *Bacillus subtillis*, *Streptococcus pneumoniae*, and *Streptococcus mutans* ($p \leq 0.05$), whereas there was no activity against Gram-negative strains in *Klebsiella pneumoniae* and *Pseudomonas aeruginosa*. Furthermore, the biofilm inhibition activity of NDG against *Pseudomonas aeruginosa* showed the least MIC of 25 µg/mL and showed the highest percentage of inhibition 96.26 with

an IC_{50} value of 12.98 µg/mL in comparison to standard antibiotics tested. The results with MRSA biofilm inhibition activity of NDG showed an IC_{50} value of 23.11 µg/mL with an inhibition percentage of 98.12 in comparison to the standard antibiotics tested. NDG showed better results in both MCF-7 and Hela cell lines with an IC_{50} of 27.15 µg/mL and 30.85 µg/mL, respectively. The NDG revealed antibacterial activity against a wide range of pathogenic bacteria and also anticancer and biofilm inhibition activity, which recognized their applications in biomedicine.

Author Contributions: Conceptualization, A.A. and R.S.; methodology, A.M. and R.S.; software, A.A., A.M. and R.S.; validation, A.A. and R.S.; formal analysis, F.M.A., M.S.A., A.L.A., M.S., R.A., S.F.A., M.K. (Mujeeb Khan) and M.K. (Mufsir Kuniyil); investigation, M.K. (Mufsir Kuniyil), R.S. and M.R.S.; resources, S.F.A. and R.S.; data curation, M.R.S. and R.S.; writing—original draft preparation, A.A., M.R.S. and R.S.; writing—review and editing, A.A., M.R.S., and R.S.; visualization, R.S., S.F.A. and M.K. (Mujeeb Khan); supervision, A.A. and R.S.; project administration, A.A. and R.S.; funding acquisition, A.A. All authors have read and agreed to the published version of the manuscript.

Funding: This research was funded by King Saud University, Riyadh, Saudi Arabia, Researchers Supporting Project number (RSP2022/R506).

Institutional Review Board Statement: Not applicable.

Informed Consent Statement: Not applicable.

Data Availability Statement: Not applicable.

Acknowledgments: The authors extend their appreciation to the Researchers Supporting Project number (RSP2022/R506), King Saud University, Riyadh, Saudi Arabia for funding this work.

Conflicts of Interest: The authors declare no conflict of interest.

References

1. Sawyers, C. Targeted Cancer Therapy. *Nature* **2004**, *432*, 294–297. [CrossRef] [PubMed]
2. Kim, S.W.; Khang, D. Multiple Cues on the Physiochemical, Mesenchymal, and Intracellular Trafficking Interactions with Nanocarriers to Maximize Tumor Target Efficiency. *Int. J. Nanomed.* **2015**, *10*, 3989–4008. [CrossRef]
3. Kwon, S.; Yoo, K.H.; Sym, S.J.; Khang, D. Mesenchymal Stem Cell Therapy Assisted by Nanotechnology: A Possible Combinational Treatment for Brain Tumor and Central Nerve Regeneration. *Int. J. Nanomed.* **2019**, *14*, 5925–5942. [CrossRef] [PubMed]
4. Bender, E. Cancer Immunotherapy. *Nature* **2017**, *552*, S61. [CrossRef] [PubMed]
5. Rhee, C.; Kadri, S.S.; Dekker, J.P.; Danner, R.L.; Chen, H.-C.; Fram, D.; Zhang, F.; Wang, R.; Klompas, M. Prevalence of Antibiotic-Resistant Pathogens in Culture-Proven Sepsis and Outcomes Associated with Inadequate and Broad-Spectrum Empiric Antibiotic Use. *JAMA Netw. Open* **2020**, *3*, e202899. [CrossRef] [PubMed]
6. Alqasim, A. Colistin-resistant gram-negative bacteria in Saudi Arabia: A literature review. *J. King Saud Univ. Sci.* **2021**, *33*, 101610. [CrossRef]
7. Almamad, M.F.; Aldujaili, N.H. Antibacterial and Antibiofilm Activity of Bacterially Reduced Graphene Oxide against Some MDR Bacterial Pathogens Isolated from Urinary Tract Infections. In *AIP Conference Proceedings*; AIP Publishing LLC: Melville, NY, USA, 2022; p. 020003.
8. Tré-Hardy, M.; Macé, C.; El Manssouri, N.; Vanderbist, F.; Traore, H.; Devleeschouwer, M.J. Effect of Antibiotic Co-Administration on Young and Mature Biofilms of Cystic Fibrosis Clinical Isolates: The Importance of the Biofilm Model. *Int. J. Antimicrob. Agents* **2009**, *33*, 40–45. [CrossRef] [PubMed]
9. Xia, T.; Fortner, J.D.; Zhu, D.; Qi, Z.; Chen, W. Transport of Sulfide-Reduced Graphene Oxide in Saturated Quartz Sand: Cation-Dependent Retention Mechanisms. *Environ. Sci. Technol.* **2015**, *49*, 11468–11475. [CrossRef] [PubMed]
10. Di Giulio, M.; Di Lodovico, S.; Fontana, A.; Traini, T.; Di Campli, E.; Pilato, S.; D'Ercole, S.; Cellini, L. Graphene Oxide Affects Staphylococcus Aureus and Pseudomonas Aeruginosa Dual Species Biofilm in Lubbock Chronic Wound Biofilm Model. *Sci. Rep.* **2020**, *10*, 18525. [CrossRef] [PubMed]
11. Papageorgiou, D.G.; Kinloch, I.A.; Young, R.J. Mechanical Properties of Graphene and Graphene-Based Nanocomposites. *Prog. Mater. Sci.* **2017**, *90*, 75–127. [CrossRef]
12. Bostan, H.B.; Rezaee, R.; Valokala, M.G.; Tsarouhas, K.; Golokhvast, K.; Tsatsakis, A.M.; Karimi, G. Cardiotoxicity of Nano-Particles. *Life Sci.* **2016**, *165*, 91–99. [CrossRef] [PubMed]
13. Hummers, W.S.; Offeman, R.E. Preparation of Graphitic Oxide. *J. Am. Chem. Soc.* **2002**, *80*, 1339. [CrossRef]
14. Alangari, A.; Alqahtani, M.S.; Mateen, A.; Kalam, M.A.; Alshememry, A.; Ali, R.; Kazi, M.; AlGhamdi, K.M.; Syed, R. Iron Oxide Nanoparticles: Preparation, Characterization, and Assessment of Antimicrobial and Anticancer Activity. *Adsorpt. Sci. Technol.* **2022**, *2022*, 1562051. [CrossRef]

15. Mohamed, M.A.; Nasr, M.; Elkhatib, W.F.; Eltayeb, W.N. In Vitro Evaluation of Antimicrobial Activity and Cytotoxicity of Different Nanobiotics Targeting Multidrug Resistant and Biofilm Forming Staphylococci. *Biomed Res. Int.* **2018**, *2018*, 7658238. [CrossRef]
16. Fais, R.; Di Luca, M.; Rizzato, C.; Morici, P.; Bottai, D.; Tavanti, A.; Lupetti, A. The N-Terminus of Human Lactoferrin Displays Anti-Biofilm Activity on Candida Parapsilosis in Lumen Catheters. *Front. Microbiol.* **2017**, *8*, 2218. [CrossRef]
17. Kalam, M.A.; Iqbal, M.; Alshememry, A.; Alkholief, M.; Alshamsan, A. Development and Evaluation of Chitosan Nanoparticles for Ocular Delivery of Tedizolid Phosphate. *Molecules* **2022**, *27*, 2326. [CrossRef]
18. Paredes, J.I.; Villar-Rodil, S.; Martínez-Alonso, A.; Tascon, J.M. Graphene Oxide Dispersions in Organic Solvents. *Langmuir* **2008**, *24*, 10560–10564. [CrossRef]
19. Vinoth, R.; Babu, S.G.; Bahnemann, D.; Neppolian, B. Nitrogen Doped Reduced Graphene Oxide Hybrid Metal Free Catalyst for Effective Reduction of 4-Nitrophenol. *Sci. Adv. Mater.* **2015**, *7*, 1443–1449. [CrossRef]
20. Kumar, M.P.; Kesavan, T.; Kalita, G.; Ragupathy, P.; Narayanan, T.N.; Pattanayak, D.K. On the Large Capacitance of Nitrogen Doped Graphene Derived by a Facile Route. *RSC Adv.* **2014**, *4*, 38689–38697. [CrossRef]
21. Acik, M.; Lee, G.; Mattevi, C.; Pirkle, A.M.; Wallace, R.; Chhowalla, M.; Cho, K.; Chabal, Y. The Role of Oxygen during Thermal Reduction of Graphene Oxide Studied by Infrared Absorption Spectroscopy. *J. Phys. Chem. C* **2011**, *115*, 19761–19781. [CrossRef]
22. Trivedi, M.K.; Dahryn Trivedi, A.B.; Khemraj Bairwa, H.S. Fourier Transform Infrared and Ultraviolet-Visible Spectroscopic Characterization of Biofield Treated Salicylic Acid and Sparfloxacin. *Nat. Prod. Chem. Res.* **2015**, *5*, 186. [CrossRef]
23. Xu, X.; Yuan, T.; Zhou, Y.; Li, Y.; Lu, J.; Tian, X.; Wang, D.; Wang, J. Facile Synthesis of Boron and Nitrogen-Doped Graphene as Efficient Electrocatalyst for the Oxygen Reduction Reaction in Alkaline Media. *Int. J. Hydrogen Energy* **2014**, *39*, 16043–16052. [CrossRef]
24. Divya, K.S.; Chandran, A.; Reethu, V.N.; Mathew, S. Enhanced Photocatalytic Performance of RGO/Ag Nanocomposites Produced via a Facile Microwave Irradiation for the Degradation of Rhodamine B in Aqueous Solution. *Appl. Surf. Sci.* **2018**, *444*, 811–818. [CrossRef]
25. Hassan, F.M.; Chabot, V.; Li, J.; Kim, B.K.; Ricardez-Sandoval, L.; Yu, A. Pyrrolic-Structure Enriched Nitrogen Doped Graphene for Highly Efficient next Generation Supercapacitors. *J. Mater. Chem. A* **2013**, *1*, 2904. [CrossRef]
26. Matsuoka, K.; Yamagishi, Y.; Yamazaki, T.; Setoyama, N.; Tomita, A.; Kyotani, T. Extremely High Microporosity and Sharp Pore Size Distribution of a Large Surface Area Carbon Prepared in the Nanochannels of Zeolite Y. *Carbon N. Y.* **2005**, *43*, 876–879. [CrossRef]
27. Wang, L.; Hu, C.; Shao, L. The Antimicrobial Activity of Nanoparticles: Present Situation and Prospects for the Future. *Int. J. Nanomed.* **2017**, *12*, 1227–1249. [CrossRef]
28. Moritz, M.; Geszke-Moritz, M. The Newest Achievements in Synthesis, Immobilization and Practical Applications of Antibacterial Nanoparticles. *Chem. Eng. J.* **2013**, *228*, 596–613. [CrossRef]
29. Huang, C.; Li, C.; Shi, G. Graphene Based Catalysts. *Energy Environ. Sci.* **2012**, *5*, 8848. [CrossRef]
30. Yang, S.; Lei, P.; Shan, Y.; Zhang, D. Preparation and Characterization of Antibacterial Electrospun Chitosan/Poly (Vinyl Alcohol)/Graphene Oxide Composite Nanofibrous Membrane. *Appl. Surf. Sci.* **2018**, *435*, 832–840. [CrossRef]
31. Huang, S.-Z.; Ma, Q.-Y.; Fang, W.-W.; Xu, F.-Q.; Peng, H.; Dai, H.-F.; Zhou, J.; Zhao, Y.-X. Three New Isopimarane Diterpenoids from Excoecaria Acerifolia. *J. Asian Nat. Prod. Res.* **2013**, *15*, 750–755. [CrossRef]
32. Hou, H.-M.; Zhu, Y.-L.; Wang, J.-Y.; Jiang, F.; Qu, W.-Y.; Zhang, G.-L.; Hao, H.-S. Characteristics of N-Acylhomoserine Lactones Produced by Hafnia Alvei H4 Isolated from Spoiled Instant Sea Cucumber. *Sensors* **2017**, *17*, 772. [CrossRef] [PubMed]
33. Chen, Y.; Lu, S.; Jia, H.; Deng, Y.; Zhou, J.; Huang, B.; Yu, Y.; Lan, J.; Wang, W.; Lou, Y.; et al. A Novel Neutralizing Monoclonal Antibody Targeting the N-Terminal Domain of the MERS-CoV Spike Protein. *Emerg. Microbes Infect.* **2017**, *6*, 1–7. [CrossRef] [PubMed]
34. Miao, J.; Lin, S.; Soteyome, T.; Peters, B.M.; Li, Y.; Chen, H.; Su, J.; Li, L.; Li, B.; Xu, Z.; et al. Biofilm Formation of Staphylococcus Aureus under Food Heat Processing Conditions: First Report on CML Production within Biofilm. *Sci. Rep.* **2019**, *9*, 1312. [CrossRef] [PubMed]
35. Neihaya, H.Z.; Zaman, H.H. Investigating the Effect of Biosynthesized Silver Nanoparticles as Antibiofilm on Bacterial Clinical Isolates. *Microb. Pathog.* **2018**, *116*, 200–208. [CrossRef]
36. Seth, A.K.; Geringer, M.R.; Hong, S.J.; Leung, K.P.; Mustoe, T.A.; Galiano, R.D. In Vivo Modeling of Biofilm-Infected Wounds: A Review. *J. Surg. Res.* **2012**, *178*, 330–338. [CrossRef]
37. Neethu, S.; Midhun, S.J.; Radhakrishnan, E.K.; Jyothis, M. Surface Functionalization of Central Venous Catheter with Mycofabricated Silver Nanoparticles and Its Antibiofilm Activity on Multidrug Resistant Acinetobacter Baumannii. *Microb. Pathog.* **2020**, *138*, 103832. [CrossRef]
38. De Lacerda Coriolano, D.; de Souza, J.B.; Bueno, E.V.; de Fátima, S.M.; dos Santos Medeiros, R.; Cavalcanti, I.D.L.; Cavalcanti, I.M.F. Antibacterial and Antibiofilm Potential of Silver Nanoparticles against Antibiotic-Sensitive and Multidrug-Resistant Pseudomonas Aeruginosa Strains. *Braz. J. Microbiol.* **2021**, *52*, 267–278. [CrossRef]
39. Vallet-Regí, M.; González, B.; Izquierdo-Barba, I. Nanomaterials as Promising Alternative in the Infection Treatment. *Int. J. Mol. Sci.* **2019**, *20*, 3806. [CrossRef]
40. Pei, X.; Zhu, Z.; Gan, Z.; Chen, J.; Zhang, X.; Cheng, X.; Wan, Q.; Wang, J. PEGylated Nano-Graphene Oxide as a Nanocarrier for Delivering Mixed Anticancer Drugs to Improve Anticancer Activity. *Sci. Rep.* **2020**, *10*, 2717. [CrossRef]